Hindawi
Mobile Information Systems
Volume 2022, Article ID 1757026, 12 pages
https://doi.org/10.1155/2022/1757026

Research Article

Mine Geological Disaster Risk Assessment and Management Based on Multisensor Information Fusion

Duo Zhang and Dongmei Feng

School of Business Administration, Liaoning Technical University, Huludao, Liaoning 125000, China

Correspondence should be addressed to Duo Zhang; zhang2126@sjzu.edu.cn

Received 29 April 2022; Accepted 30 May 2022; Published 14 July 2022

Academic Editor: Muhammad Muzammal

Mining excavation is often the main cause of geological disasters in people's construction activities. The geological disasters have the characteristics of large destruction, wide range of harm, and large loss. In particular, the collapse and slide geological disasters caused by underground mining are particularly prominent, and they have triggered a number of major natural disaster events. Therefore, it is particularly important to assess the exposure to geological hazards in mines. The purpose of this article is to study and analyze the assessment and management of the risk of geological hazards in mines based on multisensor data integration. This paper first introduces the process of multisource information fusion, and in the process of information fusion, the sensor needs to collect signals first, then preprocesses the signals provided by the sensor, and then analyzes the fusion process of D-S evidence theory algorithm and BP neural network algorithm in multisensor. Finally, the deformers in the study area are investigated by multisensor data integration techniques, the deformation and damage features of the deformers in the study area are evaluated, and the risk assessment and vulnerability evaluation of the key slopes are carried out. The experimental results of this paper show that according to the statistics of the distribution of slope disaster points, the geological disasters are mainly concentrated in 10–25°, a total of 361, accounting for 58.1% of the total disaster points. From the point density distribution, geological disasters are most concentrated at 20–30°, and the point density is 35 places/100 km^2. The results show that in areas with large slope and height difference, it is easy to form air surface, deformation, and damage, resulting in geological disasters.

1. Introduction

Geological disasters mainly involve collapses, landslides, debris flows, and so on and are widely spread all over the world. In the past decades, the frequency and intensity of geological natural disasters have increased sharply. Almost every country or region has experienced serious geological accidents, especially in developed countries. Geological disasters gravely endanger human life and assets and inflict huge damage to the natural environment. It also restricts the people's sustainable growth of economy and society. At the same time, for the risk decision of mine collapse and slide geological disaster, we should not only consider the risk source of the mine itself but also consider the planning around the mine. It gives full play to the benefits of mine geological disaster control engineering in risk control engineering, meets the requirements of social development planning, and maximizes economic and social benefits. It can be seen that how to reasonably prevent and control geological disasters and reduce people's life safety and losses caused by hydrological natural disasters as much as possible is a long-term and urgent task in front of people. We must find a more reasonable way to deal with it.

The theoretical basis of geological disaster prevention and planning is mainly the regional planning of geological disaster risk areas, while ignoring the natural vulnerability and geological risk assessment of the affected subjects. As a result, there is a great difference between the prevention and control planning of geological disasters according to the current geological risk assessment report and the actual situation. On the basis of multisensor data integration, this article studies and analyzes the risk assessment and

management of geological hazards in mines. Through risk assessment, we can gradually delineate high-, medium-, and low-risk areas, which is of great significance to the development and utilization of resources, the reduction of natural disasters, the optimization of resources, the harmonious coexistence of man and nature, and so on. At the same time, it carries out case analysis and method verification of risk evaluation and management of individual geological disasters in the mining area so as to provide new ideas for risk management of landslide geological disasters in the mining area.

Geological disaster risk decision-making is the choice of management methods after predicting the possible impact of geological disasters and finally completes the process of geological disaster risk management. The purpose of this paper is to study and analyze the risk estimation and manage the mining geohazards on the basis of multisensor data integration technology. The quantitative distribution of disaster points on the slope shows that geological disasters are mainly concentrated in 10–25°, a total of 361, accounting for 58.1% of the total disaster points. It shows that in the area with relatively large elevation difference and steep slope, it is very easy to form free surface, which will lead to geological disasters.

The innovations of this paper are as follows: (1) this paper introduces the process of multisource information fusion; (2) this paper analyzes the fusion process of D-S evidence theory algorithm and BP neural network algorithm in multisensor; and (3) through the multisensor information fusion technology to investigate the deformed body in the study area, this paper carries out the risk evaluation and vulnerability evaluation of key slopes.

2. Related Work

According to the research progress abroad, different researchers have also had corresponding cooperative research on the geological hazards of mines. Jian took Yuxi City as a case study area. Based on the sensitivity of regional geological hazards, he adjusted the resistance surface according to different types. Finally, he used the least accrued drag rate model to determine the eco-corridor and establish the guarantee model for ecological construction in Yuxi City [1]. The purpose of the Weiguo study was to investigate the precision and dependability of multiple regression approaches used for geohazard vulnerability assessment. It includes linear regression, spatial autoregression, geographically weighted regret, and support vector regret, and these methods are widely discussed [2]. Geological disasters occur frequently in the Three Gorges reservoir area of the Yangtze River Economic Zone. Yao et al. [3] proposed a program for dynamic choice of geological hazard response scenarios on the basis of case inference and foreground theories [3]. Li et al. [4] have established a monitoring and early warning platform based on SOA architecture. It integrates real-time monitoring data such as disaster early warning service and geographic information and has good service compatibility and scalability. The platform displays the real-time monitoring data of disaster-related information. They access the early warning model service in WebGIS to realize disaster early warning [4]. Zhang et al. [5] provided a three-D monitoring model of geological disasters such as landslide based on BIM. They used the real-time data iteration, incremental processing, and modeling reconstruction of geometric modeling database to form the BIM modeling dynamic response mechanism of geological hazards. They also carried out the dynamic change and adjustment of 3D landslide modeling [5]. Huang et al. [6] chose nine kinds of risk factors, such as geomorphology, geology, natural calamity, weather and hydrology, and human life. Then, the GIS method was used to analyze the spatial influence law of geological hazards and the factors synthetically and [6] was analyzed. However, these scholars still lack some technical demonstration on the research of geological hazards. It is found that the risk assessment of mine geological disasters based on multisensor information fusion has a certain reliability. For this, we consulted the relevant literature on multisensor information fusion.

Some scholars also have corresponding research on multisensor information fusion. Liu et al. [7] presented a novel multisensor data integration failure detection approach on the basis of BP neural network and D-S evidence theories [7]. To meet the obstacle guidance demands of driverless surface vehicles in complicated settings, Lv et al. [8] designed a fuzzy neural network based on multisensor data integration for obstacle guidance evolution [8]. Yang and Na [9] proposed an intelligent obstacle avoidance system based on multisensor in uncertain environment. They sensed the obstacle information through the sensor and carried out the simulation test with MATLAB simulation software [9]. Dynamic barrier recognition is crucial to ensure the autonomous movement of farming bots in unstructured environments. Liu et al. [10] proposed a method for dynamic barrier recognition using multisensor data integration [10], choosing a radar device, an inertial measure cell, and a 2D liver detector as the external sensors of the system. However, these scholars did not study and analyze the risk assessment and management of mine geological disasters based on multisensor information fusion but unilaterally discussed its significance.

3. Method

Although geological disaster risk analysis and evaluation is only a fundamental work involving disaster problems, it is indispensable in formulating disaster emergency plans. This makes the positioning of geological disaster risk assessment not only a cutting-edge scientific problem but also an important practical problem in formulating disaster prevention and reduction plans. The purpose of this article is to analyze and discuss the risk estimation and management of geological hazards in mines through multisensor data integration techniques.

3.1. Multisource Information Fusion Process. In order to realize the subsequent data exchange with the computer, the process of information fusion first needs the sensor to collect

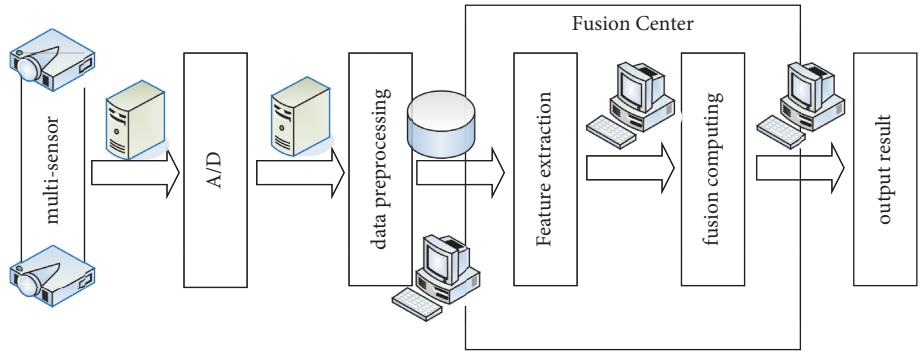

Figure 1: Multisource information fusion process.

the signal. Then, it preprocesses the signal provided by the sensor and extracts the eigenvalue and eigenvector from the preprocessed data vector. It applies appropriate fusion algorithm to fuse feature vectors [11].

In the process of data acquisition and A/D conversion, it is inevitable to be disturbed by noise. The obtained signal contains noise signal, so the digitized signal needs to be filtered to remove the noise signal before data fusion. It extracts the features of the retained signals and then fuses the feature quantities to realize the final monitoring and recognition [12].

Signal acquisition: it can obtain a variety of sensor information by various means and select different sensors to obtain the information of the measured object according to various conditions. The nonelectric quantity information is converted into the electrical signal that can be accepted by the A/D converter port, and the electrical signal information is converted into the current information that can be accepted by the computer I/O port [13].

Signal preprocessing: there is noise in the measured information, and the transformed discrete-time information is more than the measurement noise of A/D converter. It must preprocess the monitoring information extracted from the sensor and increase the signal-to-noise ratio to realize information fusion of the data [14]. We can also realize information preprocessing through zero mean, filtering, removing outliers, and other steps.

It extracts the features of the information monitored by the sensor.

Fusion Computing: because there has been a lack of systematic basic research architecture in the field of multisensor information fusion, fusion research is usually carried out according to the specific problems in an application field. Therefore, when dealing with specific problems, fusion technology can be selected according to the fusion objectives and data characteristics [15]. Figure 1 is the schematic diagram of the information fusion process.

3.2. Algorithm Based on D-S Evidence Theory. In order to realize target recognition and attribute decision, it can infer based on these uncertain information and data fusion. There are many uncertain reasoning methods. Among them, the D-S evidence model plays an important role in the representation of uncertainty, the calculation, and the combination of uncertainty, so it plays an important role in the fusion algorithm. It can be seen that the process of dealing with information and data with poor integrity, strong uncertainty, and unclear data is an uncertain reasoning process and the basis of target recognition.

Basic Probability Distribution Function: the basic probability distribution method assigns a probability value to all subsets in the framework. This probability is often described by mass function. The basic probability distribution function can be used to characterize the trust degree of each evidence body. Let θ be an identification framework, 2^θ be the set of all subsets of θ, and the mapping $q(X)$: $2^\theta \longrightarrow [0,1]$ meets the following conditions:

$$\begin{cases} \sum_{X\subseteq\theta} q(X) = 1, \\ q(\varnothing) = 0, \\ 0 \le q(X) \le 1. \end{cases} \tag{1}$$

Q is the basic probability distribution function on 2^θ, which is called the mass function, and $Q(x)$ is called the basic probability number. When $Q(x) > 0$, X is the focal element, and the number of elements contained in the focal element is the basis of this focal element. $Q(x)$ represents the most accurate part of hypothesis X and is the direct support for X. In addition to the exact letter to x, the most accurate letter to any subset of X must be calculated so that $q_1, q_2, q_3, \ldots, q_p$ becomes the focal element, which uses the trust function.

Trust Function: under the complete recognition framework θ, for all $X \subset \theta$, $Y \subseteq X$, the trust function Bel: $2^\theta \longrightarrow [0,1]$ of the proposition satisfies the following formula:

$$\mathrm{Bel}(X) = \sum_{Y\subseteq X} q(Y). \tag{2}$$

Bel function is called trust function, also known as lower bound function, and it can be expressed as the sum of basic probability distributions of all subsets in set X. It well expresses the degree of support for proposition x, including its subset $\mathrm{Bel}(\varnothing) = 0$, $\mathrm{Bel}(\theta) = 1$.

Likelihood Function: the likelihood function can also be called the upper limit function or the nonrefutation function. The relationship between the likelihood function $Pl(X)$ and the trust function Bel (X) is illustrated in Figure 2.

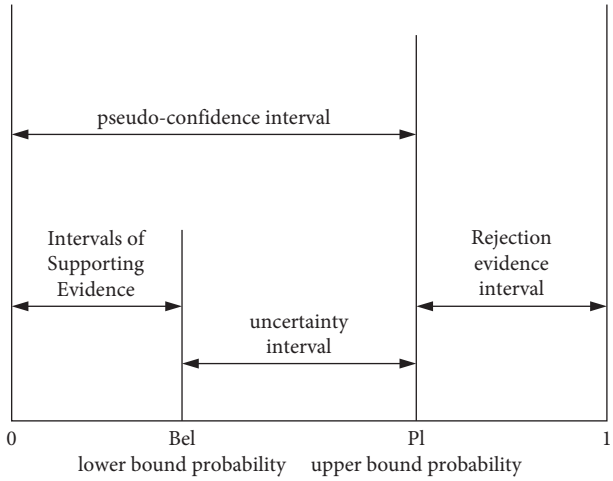

Figure 2: Schematic diagram of trust interval.

In order to express the trust degree of X more accurately, it uses the likelihood function $Pl(X)$ to describe the nonfalse trust degree of X. If we know that Bel (x) represents the degree of trust in proposition x as true, then Bel (x) represents the degree of trust in X as false. Therefore, $Pl(x)$ represents the degree of trust in X as nonfalse as shown in the following formula:

$$Pl(X) = \sum_{Y \cap X \neq \varnothing} q(Y). \tag{3}$$

Under the framework of recognition, for event X, the likelihood function $Pl(X)$ and trust function Bel (X) can be obtained by the basic probability assignment function. We can use [Bel (X) and Pl (X)] to represent the uncertainty interval of this event. The ratio between the trust function and the likelihood function is $Pl(X)$ − Bel (X), which describes the uncertainty of X.

Synthesis Rules and Decision-Making Methods of D-S Evidence Theory: synthesis rules: in application, for the same evidence body, the sources may be different, resulting in different probability distribution functions. At this time, it is necessary to synthesize these probability distribution values. Let q_1 and q_2 be two different probability distribution functions, and their orthogonality and formula are as follows:

$$q = q_1 \oplus q_2. \tag{4}$$

The following conditions are met:

$$\begin{aligned} q(\varnothing) &= 0, \\ q(X) &= L^{-1} \times \sum_{Y \cap Z = X} q_1(Y) \times q_2(Z). \end{aligned} \tag{5}$$

The coefficient L^{-1} is a normalization factor, which can prevent the nonzero probability from being assigned to the empty set during the synthesis operation, and the coefficient is as follows:

$$L = 1 - \sum_{Y \cap Z = \varnothing} q_1(Y) \times q_2(Z). \tag{6}$$

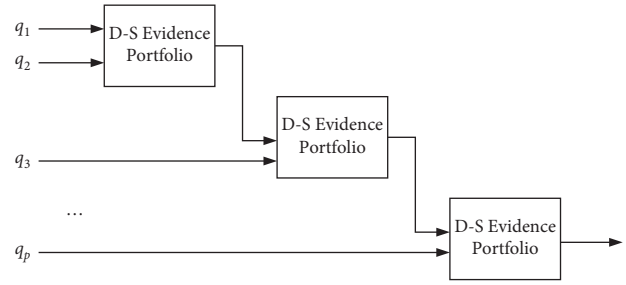

Figure 3: Recursive structure of multiple evidence combinations.

If $l = 1$, it means that the two evidences are completely consistent, i.e., compatible; when $L = 0$, L^{-1} is meaningless, and orthogonality and Q do not exist, indicating that q_1 and q_2 completely conflict, that is, the two evidences are contradictory; when $L \neq 0$, then the orthogonal sum q is a new probability distribution function. The evidence conflict coefficient is

$$L' = \sum_{Y \cap Z = \varnothing} q_1(Y) \times q_2(Z). \tag{7}$$

The contradiction coefficient represents the degree of contradiction between the two kinds of evidence. The above formula is also called Dempster's rule of evidence synthesis.

When the synthesis conditions are met, the orthogonal sum operation of multiple probability distribution functions is as follows:$\forall X \subseteq \theta$, supposing $q_1, q_2, \ldots, q_p$ is p probability distribution functions on the recognition framework θ, then the orthogonal sum $q = q_1 \oplus q_2 \oplus \cdots \oplus q_p$ of these functions.

$$q(X) = L^{-1} \times \sum_{X_1 \cap X_2 \cdots \cap X_p = X} \prod_{1 \leq n \leq p} q_n(X_n), \tag{8}$$

L^{-1} is the normalization factor, and the sequence of evidence combination has no effect on the synthesis result. The probability distribution function is recursively combined by the Dempster evidence combination rule as shown in Figure 3.

In essence, the procedure of proving inference is to accumulate evidence by using orthogonal algorithm so as to constantly change people's trust in hypothesis and reduce the degree of belief in incorrect hypothesis.

Fusion Process of Evidence Theory: Figure 4 shows the convergence process of D-S evidence theory. First, the information obtained from each sensor is preprocessed. To satisfy the conditions for applying Dempster's evidence combination rule, the underlying probability allocation function (BPA) and the confidence function (BEL) are calculated for every evidential body. It is also ensured that there is no conflict among the evidence bodies, i.e., they are independent of each other, and then, the probability distribution functions of multiple evidence bodies are combined using the D-S combining rule to obtain a new evidence body. The closer the underlying odds ratio definition function of the new body of evidence is to 1, the higher the accuracy of the proposition's judgment and the greater the support for the proposition to be true. Finally, certain decision rules are used to select the outcome with the least uncertainty.

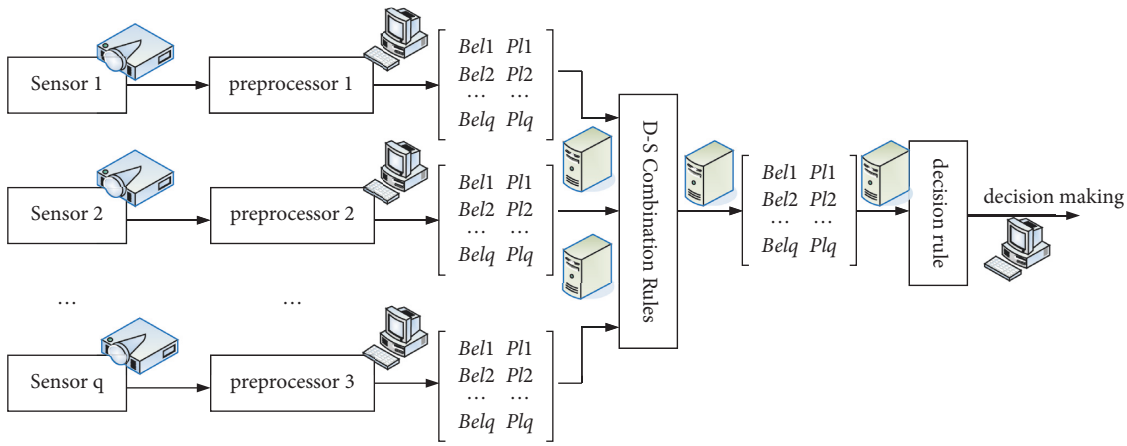

Figure 4: D-S fusion process of evidence theory.

3.3. BP Neural Network Fusion Algorithm. Structure Design of BP Neural Network: the efficiency and characteristics of the BP network are directly related to its network structure design, selected training and learning samples, activation function, practice times, and learning rate.

Data Selection: the sample is the feature vector used for subsequent training. It is necessary to select meaningful data that can represent the nature of the event. The types of samples are not the more the better. Too much will increase the amount of training. In order to prevent the difference in sensitivity to different data after training, the weight of each type of sample selected must be the same; otherwise, the overall accuracy will be reduced. At the same time, the risk of the local infimum point of the network is also great.

Design of Input Layer and Output Layer: the dimension of input data is determined by the total number of neurons in the input layer of the BP network, and the total number of neurons in the input and output layer is determined according to the classification number of expected transmission signals.

Hidden Layer Design: correctly setting the number of hidden layers is the key step of hidden layer design. The more the times of hidden layers, the lower the calculation error rate of the neural network. However, the more the layers, the more complex the neural network is, and the longer the training duration is, and the problem of over fitting will occur. It has been proved that assuming that the entry layer and output layer in the neural network use linear transformation function, and the covert layer uses S-type change function, only one covert layer in the neural network can approach a rational function infinitely. In order to reduce the complexity of the network and reduce the training time, the network structure with only one hidden layer should be considered first when designing BP neural network. The error can be reduced by increasing the number of neurons in the hidden layer. However, it does not mean that the more neurons in the hidden layer, the better. We need to set the number of neurons appropriately in combination with experience. The commonly used empirical formula is as follows:

$$k = \sqrt{p+q} + l, \tag{9}$$

where p represents the total number of neurons in the entry level, k represents the total of neurons in the hidden level, q represents the total of neurons in the export level, and l is a constant greater than 0 and less than 10.

The Initial Set of Weights: the error function has a local minimum value, so the BP neural network algorithm converges to the local maximum or global minimum point and also converges to a very small point determined by the initialization size of the network, so the setting of the weights is very important. Therefore, if the sigmoid conversion function is used in the neural network, based on the characteristics of this function, if it wants to get better fusion results, the initial connection weight should be set between −0.5 and 0.5.

Selection of Activation Function: most networks use sigmoid function, so it requires that the activation function meeting the requirements of BP algorithm must be continuously differentiable:

$$g(a) = 1 + \frac{1}{1+e^{\varphi a}}. \tag{10}$$

The convergence rate of the activation function decreases with the increase in φ, and the curve is more gentle; on the contrary, the smaller the φ value, the faster the convergence rate, and it is likely to fluctuate near the extreme point.

BP Neural Network Fusion Process: learning process: the key to the learning of the BP neural network is to dynamically adjust the connection weights by importing the sample data of the system, and then repeatedly adjusting the link weights between all levels in the network, so as to improve the mapping relationship of all levels and finally make the network data close to the expected data as much as possible. In the process of machine learning, the link weights of all levels must be adjusted under the condition of abiding by some adjustment principles, but not arbitrarily. Its core idea is that each neuron at all levels shares the output error and then passes back to the hidden layer and input layer step by step so as to adjust the weight of each unit. The direction of error

back propagation is that the error is represented in each layer in some form—correcting the weight of each layer unit.

The input data between the interneurons of each layer of the BP neural network is shown as neuron n in the input level. The input data are shown for neuron n in the input level:

$$\text{net}_n = \sum_{n=1}^{Q} a_n + \varphi_n. \tag{11}$$

Its output function is

$$x_n = g(\text{net}_n). \tag{12}$$

$g()$ is an S-type function and φ_n is the threshold set in the input layer.

The input data of neuron m in the hidden layer is expressed as follows:

$$\text{net}_m = \sum_{m=1}^{P} v_{nm} x_m + \varphi_m. \tag{13}$$

Its corresponding output function is

$$x_m = g(\text{net}_m). \tag{14}$$

The input function of neuron h in the output layer is expressed as follows:

$$\text{net}_h = \sum_{h=1}^{R} v_{mh} x_m + \varphi_h. \tag{15}$$

Its corresponding output function is

$$b_h = g(\text{net}_h), \tag{16}$$

where v_{mh} is the weight of the output layer and φ_h is the set threshold.

BP Algorithm Weight Adjustment: it uses the gradient steepest descent method to estimate the opposite deviation information. The opposite deviation information CC statistical formula of the output layer is expressed as follows:

$$\gamma_h = (b_{th} - b_h) g(\text{net}_h) = b_h (1 - b_h)(b_{th} - b_h). \tag{17}$$

The calculation formula of the reverse error signal γ_m of the hidden layer is

$$\gamma_m = x_m (1 - x_m) \sum_{h=1}^{K} \gamma_h v_{mh}. \tag{18}$$

On the basis of the error, the two formulas are used to calculate the weight difference between the middle layer and the output layer.

$$\begin{aligned} v_{nm}(h+1) &= v_{nm}(h) + \tau_m \gamma_m x_n + x_n \left(v_{nm}(h) - v_{nm}(h-1)\right), \\ v_{mh}(h+1) &= v_{mh}(h) + \tau_h \gamma_h x_m + x_m \left(v_{mh}(h) - v_{mh}(h-1)\right). \end{aligned} \tag{19}$$

In the two formulas above, x is the memory factor, which is the coefficient that each layer changes the weight of the link in the past and the degree of influence on the current link weight changes. τ is the learning speed coefficient.

When BP and neural networks are fully integrated with each other, first preprocess the output signals of each sensor, then comprehensively process the trained data analysis, and finally get the decision signal output.

4. Experimental Results and Analysis

Overview of Area: the research case selected in this paper is the Houshan deformation body of a coal mine.

Due to the mining engineering activities of coal mine, a large number of deformation and damage phenomena occur in the back mountain of the coal mine plant, especially the deformation of the mountain in the upper part of the goaf, which is likely to be unstable. This poses a great threat to the lives, property, and engineering construction of the people at the foot of the mountain. Therefore, this paper investigates the deformed body in the study area through multisensor information fusion technology and analyzes the deformation and failure characteristics of the deformed body in the study area. It carries out the risk assessment and vulnerability assessment of key slopes and finally realizes the risk assessment of the back mountain deformation body of a coal mine. It also puts forward corresponding risk management methods according to the characteristics of the geological environment in the study area, which provides new disaster prevention and reduction countermeasures for mine safety.

4.1. Deformation and Instability Characteristics of Slope Based on Physical Simulation Technology. For the physical simulation experiment of rock materials, the determination of similarity constant and the selection and proportion of similar materials have a significant impact on the physical and mechanical properties of materials. The closer the physical and mechanical properties of similar materials are to the actual rock mass, the more authentic the results obtained from the simulation experiment are. This slope is an anti-inclined rock slope, and the main reference failure forms are tension crack and shear. Therefore, the similarity of stress in the test mainly considers the similarity of shear strength of rock mass.

Determination of Physical and Mechanical Parameters of Rock and Soil Mass: sandstone, strongly weathered sandstone, and thin mudstone are mainly distributed in the study area. This test mainly considers the physical and mechanical properties of sandstone, so the rock samples collected on-site are mainly fresh sandstone and strongly weathered sandstone in two large landslide deposits. In this paper, 18 fresh sandstones and 12 strongly weathered sandstones are selected for point load and direct shear tests, respectively, and the rock mechanical parameters are finally determined as shown in Table 1.

Orthogonal Test: the orthogonal test mainly considers three levels and two factors, which are the mass ratio of bonding material/aggregate and barite/quartz sand. The bonding material is gypsum, and barite and quartz sand are aggregates. Based on the analysis of the test data of the direct shear test, the change in total mass ratio and aggregate mass ratio has an impact on the mechanical properties of the

Table 1: Test values of rock strength parameters.

Lithology	Sandstone	Strongly weathered sandstone
Internal friction angle (°)	37.9	32.1
Tensile strength (MPa)	12.91	9.89
Uniaxial compressive strength (MPa)	96.99	53.97

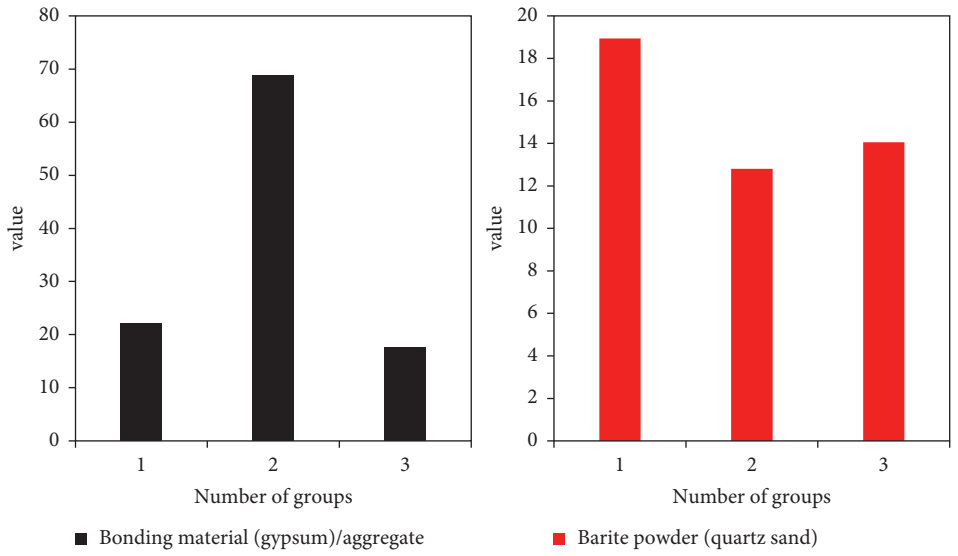

Figure 5: Analysis of cohesion sensitivity factors.

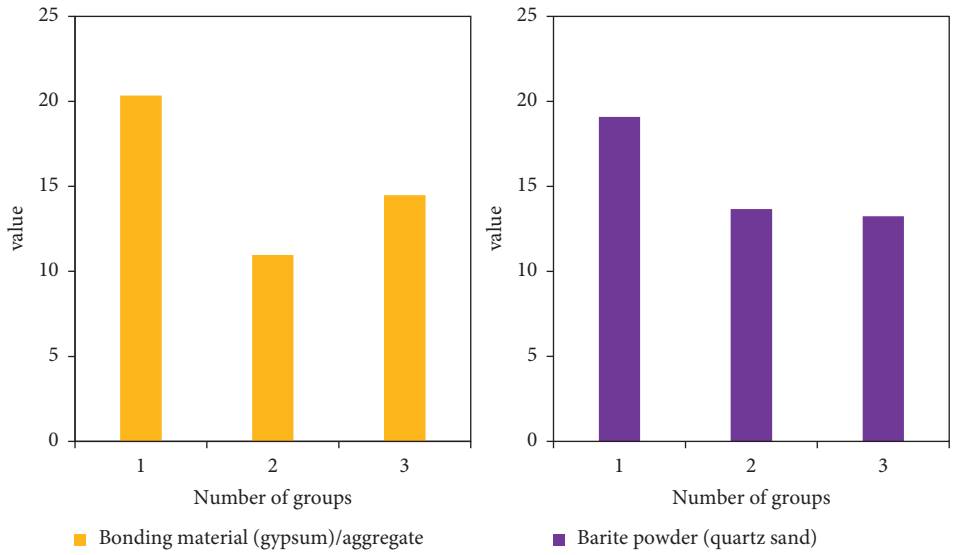

Figure 6: Analysis of sensitivity factors of internal friction angle.

sample, but the degree of impact is different. Therefore, it is necessary to analyze the sensitivity of influencing factors of mechanical parameters.

Sensitivity of Influencing Factors of Cohesion: in this paper, the average value and range of each level of the factors affecting the cohesion of the sample in the orthogonal test are obtained, and the results are shown in Figure 5. It can be seen that the range of bonding material (gypsum)/aggregate ratio factor is large, which plays a main control role in the sample. Due to the increase in this ratio factor, the cohesion increases before and decreases after. Among them, the effect of the barite powder/quartz sand ratio is relatively small. Since the cohesion value of the proportioning material to be selected is small, the value with small factor ratio of the bonding material (gypsum)/aggregate is selected as the main control value. The parameters are adjusted by increasing or decreasing the ratio of barite powder to quartz sand.

Table 2: Classification of different landslide factors table.

Relevant factors	Name category	Disaster points	Percentage (%)
Material composition	Soil quality	569	96.69
	Rock quality	16	2.54
Slide body thickness	<5 m	509	86.69
	5 ~ 10 m	59	10.58
	10 ~ 15 m	10	1.41
	>15 m	3	0.66
Form of exercise	Push type	45	7.38
	Traction type	539	92.78

Table 3: Classification of different landslide factors table.

Relevant factors	Name category	Disaster points	Percentage (%)
Current stability	Unstable	131	22.01
	Basically stable	439	74.99
	Stabilize	20	3.27
The size of the landslide	Extra large	2	0.2
	Large	6	0.8
	Medium	71	11.51
	Small	509	87.49

Sensitivity Analysis of Influencing Factors of Internal Friction Angle: the mean values of the factors affecting the internal friction angle of the samples in the orthogonal experiments and the extent of each rank were obtained, and the results are shown in Figure 6. It can be seen that the bonding material (gypsum)/aggregate ratio factor also plays a major control role in the sample, and the barite powder/quartz sand ratio factor takes the second place. Therefore, the bonding material (gypsum)/aggregate ratio factor shall be determined first, and then, the ratio of barite powder/quartz sand shall be adjusted.

Analysis of Test Results: at the beginning of the test, after the instrument operated for a period of time, discontinuous small tensile cracks appeared on the surface of the upper slope and in the rock stratum. It shows that without any reinforcement measures in the goaf, it has a certain impact on the rock stratum in the upper part of the slope, and the mining of the coal seam in the lower part loses the support to the upper rock stratum. Tensile stress is generated in the upper rock stratum under the action of gravity, resulting in tensile cracks in the rock mass at local positions.

With the progress of the test, the tension crack in the upper rock mass of the goaf gradually expanded, and the interlayer tension failure began to appear on the slope surface. The slope surface has local collapse and falling.

With the deformation and destruction of the rock body on the above side slope, the collapse and destruction of the quarry area gradually intensified. The tension cracks developed on the surface of the slope gradually extended to the upper part of the slope, and the rock at the top of the cobble was affected by the laminated structure. It gradually falls onto the cobbles and accumulates at the bottom of the area.

Finally, the rock mass in the upper part of the goaf completely collapsed.

4.2. Basic Types and Characteristics of Landslide Geological Hazards. The landslide is preliminarily divided according to the material composition, thickness, sliding mechanical mechanism, stability, and scale of the landslide. The results are shown in Tables 2 and 3.

It shows that the landslides are mainly small and medium-sized landslides, accounting for 99% of the total number of landslides. At present, the landslide is basically stable, accounting for 74.99%. The movement form of landslide is mainly traction type, accounting for 92.78% of the total number of landslides. Most of them are soil landslides, accounting for 96.69% of the total number of landslides. At the foot of the slope, the thickness of loose soil is relatively large, which is easy to produce soil deformation and fragmentation. Therefore, the sliding of loose soil along the contact surface with bedrock is the main form of soil sliding in the working area.

According to the time statistics of geological disasters or signs of deformation, among the 621 geological disasters in the region, 3 in February, 5 in April, 11 in May, 28 in June, 209 in July, 82 in August, 264 in September, and 19 in October have deformation and damage. The temporal distribution of geological disasters in the working area is shown in Figure 7.

4.3. Spatial Distribution Characteristics of Geological Hazards. Geological Hazard Features in Terrain and Landforms: 621 geological hazard points in the working area are counted according to the distribution of different types of landform, and the statistical results are summarized in Table 4.

The analysis and statistics show that geological disasters mainly occur in low-mountainous and hilly areas, with a total of 620, accounting for 99.8% of the total disasters. In low-mountainous areas, disasters are mainly distributed in

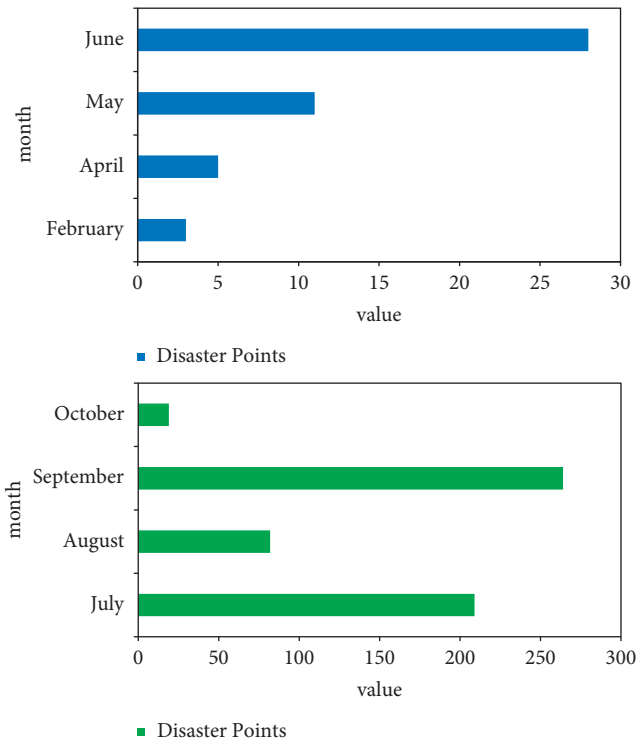

Figure 7: Statistical chart of months of geological disasters.

Table 4: Statistical table of relationship between geological hazards and landform.

		Types and quantities of geological hazards				
		Landslide	Collapse	Debris flow	Total	Proportion (%)
Middle mountain	Middle cut mountain	1	—	—	1	0.15
Low mountain	High platform and low mountain	24	—	—	24	3.69
	Canyon low mountain	287	10	2	272	43.59
	Narrow valley and low mountain	169	18	—	187	30.39
Hilly area	Ridge	116	9	—	125	19.97
	Mid cut	11	—	—	11	2.11

the stepped wide mountain canyon low-mountain area, with 272 geological disasters, accounting for 13.63% of the total landslides. The area density of geological hazards in ridge-wide valley hilly terrain of hilly area is the highest, up to 51.59 places/100 km^2. Therefore, geological disasters in these areas are relatively developed. The density of hydrological disasters in hilly areas is higher than that in low areas. It can be seen that the development of geological disasters in the working area is not only controlled by the topographic and geomorphic conditions but also active human work and has a great negative impact on the growth and development of geological disasters. The hilly area within the county planning has a large population accumulation. It is also greatly affected by people's construction social activities and environment, so the distribution density of geological disasters is also great.

The statistics on the distribution of disaster points on the slope show that in terms of quantity distribution, geological disasters are mainly concentrated at 10–25°, with a total of 361, accounting for 58.1% of the total disaster points. In terms of point density distribution, geological disasters are most concentrated at 20–30°, and the point density is 35 places/100 km^2. Figure 8 shows the distribution law of slope and disaster points (Figure 8(a)) and the distribution law of relative elevation difference and disaster points (Figure 8(b)). The height difference refers to the relative height of the slope, that is, the slope height. The height difference is classified and counted according to the interval of 10 m. The statistical results show that the disaster points are mainly distributed in the range of 10–40 m height difference, accounting for 74.8% of the total number of disaster points. The disaster point density is the highest in the range of 50–70 m, reaching 40 places/100 km^2. The total data show that the free face is easy to form in the area with steep slope and relatively large elevation difference. It is prone to deformation and damage and geological disasters.

Distribution Characteristics of Geological Hazards with Rainfall: rainfall is the main inducing factor of geological

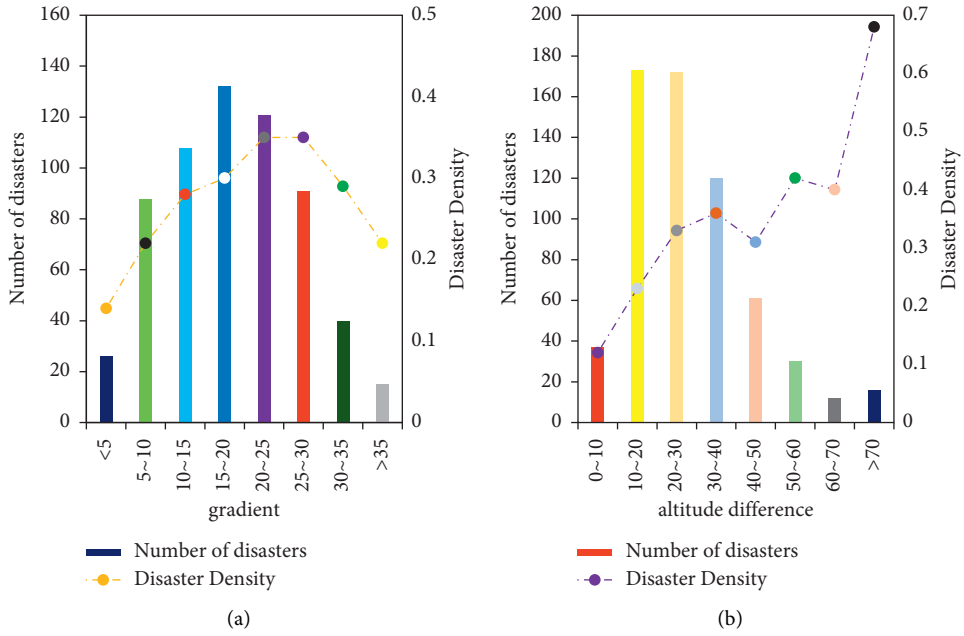

Figure 8: Distribution law of slope and disaster points, relative elevation difference, and disaster points.

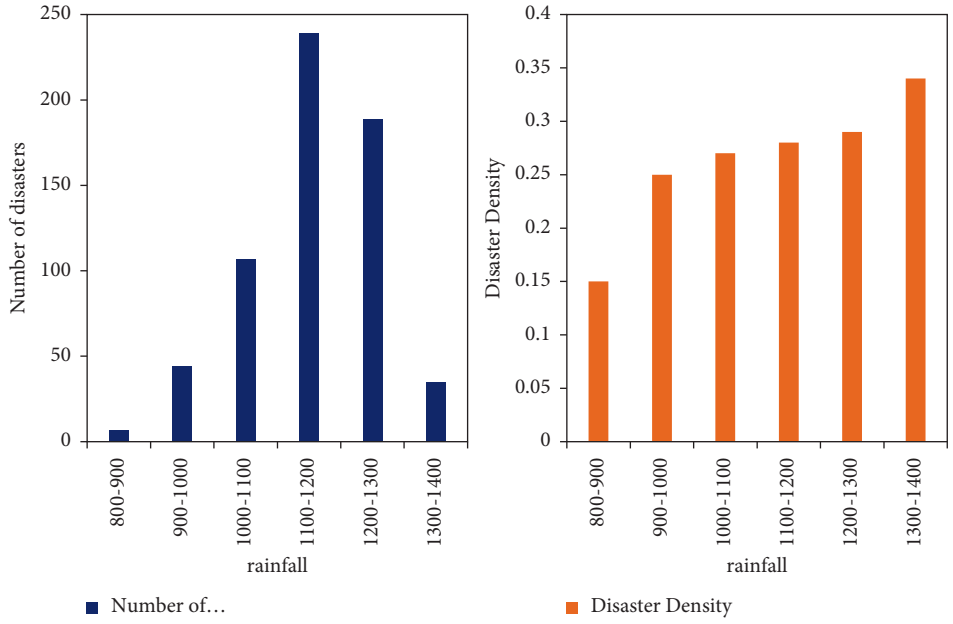

Figure 9: Distribution law of rainfall and disaster points.

disasters. The amount of rainfall directly affects the number of disasters. The average rainfall varies greatly, with 1130–1782.8 mm in the northeast, 1100–1170 mm in the middle, and 1035–1230 mm in the southwest. The whole county is divided into 6 sections according to the 100 mm section. The statistical results of the number of disaster points in different levels of rainfall are shown in Figure 9.

The data show that the number of disaster points in the range of 1100 mm–1300 mm is as high as 428, accounting for 68.9% of the total disaster points. The disaster point density is the largest in the range of 1300–1400 mm, up to 34/100 km^2, and 35 disaster points. After analysis, this is due to the relatively small land area in the range of 1300–1400 mm. Therefore, the density of disaster points is large, and on the whole, the density of disaster points is positively correlated with the increase in rainfall.

Distribution Characteristics of the Relationship between Geological Hazards and the Distance between Rivers and Roads: since human development, human daily life is closely related to rivers. Roads are built along the river, and houses are built along both banks of the river, which not only brings convenience to mankind but also brings disaster. Through

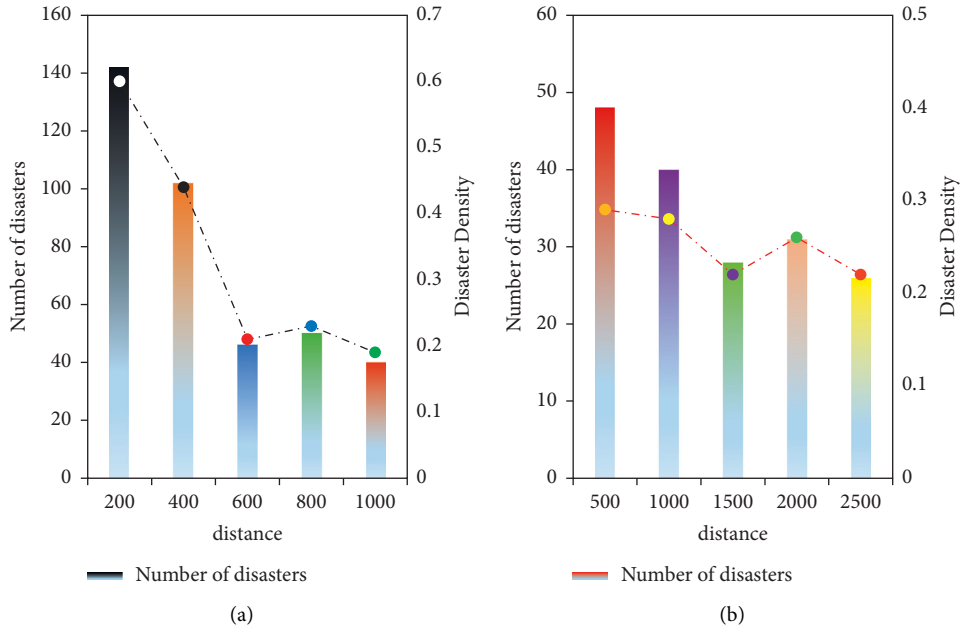

Figure 10: Statistical diagram of the relationship between water system and disaster points and between human engineering and disaster points.

the statistics of disaster point data in different ranges from the river, Figure 10(a) is obtained in this paper.

The statistical results show that the river distribution plays an obvious role in controlling the development of landslide geological hazards. The number of disaster spots gradually decreases with the increase in distance from the river. According to the analysis of statistical results, landslide geological hazards are most distributed when the distance from the water system is $d \leq 200$ m, and the density of disaster points is 60/100 km^2. The distance from the point of landslide disaster to the point of water system is less than or equal to 200 m, and the density of landslide disaster is less than or equal to 1000 m.

On the one hand, the construction of roads is conducive to people's travel and social development. It also damaged the environment and the original landform in different degrees during the construction and affected the stability of the slope. Therefore, it is also closely related to the occurrence of disasters. Through the statistics of the number of disaster points in different ranges on both sides of the road, the results are shown in Figure 10(b).

The statistical findings show that road distribution has a clear effect on controlling the growth of landslide geological hazards. The number of disaster sites gradually decreases as the relationship with the road increases. According to the analysis of statistical results, landslide geological hazards are distributed most at a distance of $D \leq 500$ m from the road, and the density of disaster points is 29/100 km^2. When the distance from the road is 500 m $< D \leq 2500$ m, the density of landslide disaster points is slightly smaller, the distance from the water system is $d > 2500$ m, and the distribution of landslide geological disasters and the density of disaster points are the least.

5. Conclusions

Multisensor information fusion can enhance the survivability of the system, improve the reliability and robustness of the entire system, enhance the credibility of the data, improve the accuracy, expand the time and space coverage of the system, and increase the real-time information utilization of the system. The purpose of this paper is to research and analyze the risk assessment and management of mine geological hazards based on multisensor information fusion. At the same time, on the basis of geological disaster risk assessment, the overall planning to reduce the loss of geological disasters or avoid the occurrence of disasters is given in a targeted manner, and the disaster areas are divided into key prevention and control areas, subkey prevention and control areas, and general treatment areas and put forward prevention and management suggestions for each control area. Specific prevention opinions are given on a single disaster site, and the research results can also be used in geological disaster prevention planning and management practice and have important guiding significance for other types of regional natural disaster prevention planning. However, due to the limitations of the times and technology, people have not carried out in-depth research on the causes of geological disasters. Therefore, this paper will carry out in-depth research and discussion in the future.

Data Availability

The data used to support the findings of this study are available from the corresponding author upon request.

Conflicts of Interest

The authors declare that they have no conflicts of interest.

Acknowledgments

This research study was sponsored by Risk Assessment of Environmental Geological Hazards in Western Open-day Mining Area, China (project no. 2017YFC1503102).

References

[1] P. Jian, N. G. Xiao, Y. Hu, and Y. X. Liu, "Constructing ecological security patterns in mountain areas based on geological disaster sensitivity: a case study in Yuxi City, Yunnan Province, China," *Ying yong sheng tai xue bao = The Journal of Applied Ecology*, vol. 28, no. 2, pp. 627–635, 2017.

[2] W. Jiang, P. Rao, R. Cao, Z. Tang, and K. Chen, "Comparative evaluation of geological disaster susceptibility using multi-regression methods and spatial accuracy validation," *Journal of Geographical Sciences*, vol. 27, no. 4, pp. 439–462, 2017.

[3] X. Yao, H.-X. Guo, J. Zhu, and Y. Shi, "Dynamic selection of emergency plans of geological disaster based on case-based reasoning and prospect theory," *Natural Hazards*, vol. 110, no. 3, pp. 2249–2275, 2021.

[4] Z. Li, X. Leng, and J. Liang, "Design of geological disaster monitoring and warning platform based on SOA," *Journal of Chengdu University of Technology (Science & Technology Edition)*, vol. 45, no. 5, pp. 606–614, 2018.

[5] C. Zhang, Z. Chen, and M. Wei, "3D monitoring of landslide geological disaster and its application based on BIM," *Journal of Chengdu University of Technology (Science & Technology Edition)*, vol. 44, no. 3, pp. 377–384, 2017.

[6] S. Huang, J. Kong, and Y. Cui, "Disasterous spatial distritution and danger zonation of secondary geological disaster in Xizhang after "4·25" M_s8.1 Nepal earthquake," *Journal of Natural Disasters*, vol. 26, no. 1, pp. 80–88, 2017.

[7] B. J. Liu, Q. W. Yang, and W. U. Xiang, "Application of multi-sensor information fusion in the fault diagnosis of hydraulic system," *International Journal of Plant Engineering and Management*, vol. 22, no. 1, pp. 12–20, 2017.

[8] J. Lv, C. Qu, C. Qu et al., "Research on obstacle avoidance algorithm for unmanned ground vehicle based on multi-sensor information fusion," *Mathematical Biosciences and Engineering*, vol. 18, no. 2, pp. 1022–1039, 2021.

[9] J. Yang and Q. Na, "Avoiding obstacle system of intelligent vehicle based on multi-sensor information fusion" IPPTA," *Quarterly Journal of Indian Pulp and Paper Technical Association*, vol. 30, no. 8, pp. 800–807, 2018.

[10] M. Liu, J. Chen, and X. Zhao, "Dynamic obstacle detection based on multi-sensor information fusion," *IFAC-PapersOnLine*, vol. 51, no. 17, pp. 861–865, 2018.

[11] J. Wang and L. Xue, "Application of K-means algorithm in geological disaster monitoring system," *International Journal of Advanced Network Monitoring and Controls*, vol. 3, no. 3, pp. 16–22, 2019.

[12] L. Yunyan and L. Na, "The comprehensive utilization of geological disaster land in mountainous cities of China," *Disaster Advances*, vol. 10, no. 3, pp. 41–47, 2017.

[13] N. Sun, H. Qin, and L. Zhang, "Vehicle target recognition based on multi-sensor information fusion," *Qiche Gongcheng/ Automotive Engineering*, vol. 39, no. 11, pp. 1310–1315, 2017.

[14] X. Xiangyu, M. Wang, L. Luo, Z. Meng, and E. Wang, "An indoor pedestrian localization algorithm based on multi-sensor information fusion," *Journal of Computer and Communications*, vol. 5, no. 3, pp. 102–115, 2017.

[15] K. Nisar, "Smart home: multisensor information fusion towards better healthcare," *Advanced Science Letters*, vol. 24, no. 3, pp. 1896–1901, 2018.